Anomalous thermal expansion in rare-earth gallium perovskites: a comprehensive powder diffraction study

2009 J. Phys.: Condens. Matter 21 145405

(http://iopscience.iop.org/0953-8984/21/14/145405)

J. Phys.: Condens. Matter **21** (2009) 145405 (14pp) doi:10.1088/0953-8984/21/14/145405

Anomalous thermal expansion in rare-earth gallium perovskites: a comprehensive powder diffraction study

A Senyshyn[1,2,8], D M Trots[1,3], J M Engel[1,4], L Vasylechko[2], H Ehrenberg[1,5], T Hansen[6], M Berkowski[7] and H Fuess[1]

[1] Institute for Materials Science, Darmstadt University of Technology, D-64287 Darmstadt, Germany
[2] Lviv Polytechnic National University, 12 Bandera Street, 79013 Lviv, Ukraine
[3] HASYLAB at DESY, Notkestraße 85, D-22607 Hamburg, Germany
[4] Institut für Werkstoffwissenschaft, Technische Universität Dresden, Helmholtzstraße 7, 01069 Dresden, Germany
[5] Institute for Complex Materials, IFW Dresden, Helmholtzstraße 20, D-01069 Dresden, Germany
[6] Institut Max von Laue–Paul Langevin, 38042 Grenoble Cedex 9, France
[7] Institute of Physics, Polish Academy of Sciences, Aleja Lotników 32/46, 02-668 Warsaw, Poland

Received 26 September 2008, in final form 11 February 2009
Published 13 March 2009
Online at stacks.iop.org/JPhysCM/21/145405

Abstract
Crystal structures of rare-earth gallium perovskites $LaGaO_3$, $PrGaO_3$, $NdGaO_3$ and $Pr_{1-x}Nd_xGaO_3$ ($x = 0.25, 0.50, 0.75$) solid solutions were investigated in the temperature range 12–300 K by high-resolution powder diffraction using synchrotron or neutron radiation. The previously reported negative thermal expansion in the *b* direction of the $PrGaO_3$ lattice has been found to be persistent in $Pr_{1-x}Nd_xGaO_3$ solid solutions and its magnitude has been revealed as proportional to the amount of praseodymium. Evaluation of the obtained temperature evolution of cell dimensions indicated a weak anomalous behaviour of the *b* lattice parameter in $NdGaO_3$, and its origin is supposed to be the same as in $PrGaO_3$, i.e. a coupling of the crystal electric field levels with phonon excitations of about 23–25 meV energy. The performed bond length analysis revealed an anomalous behaviour of both LnO_{12} (Ln—rare-earth) and GaO_6 coordination polyhedra, which can be a structural manifestation of anomalous thermal expansion in the considered compounds.

(Some figures in this article are in colour only in the electronic version)

1. Introduction

Perovskite-type rare-earth gallates have attracted considerable interest from researchers for a long time due to their attractive properties. The best known application of these materials is their use as substrates for colossal magnetoresistive manganates, $Sr(Pb)TiO_3$, GaN [1] and high-temperature cuprate superconductor films [2, 3], where good matching of lattice parameters for both film and substrate makes the growth of buffer layers non-mandatory. Recently $LaGaO_3$, $NdGaO_3$ and $PrGaO_3$, doped with alkaline-earth elements, have been reported as suitable electrolytes in solid oxide fuel cells [4–6].

It is obvious that the development of applications based on these materials requires extended and accurate knowledge of their crystal structures and their behaviour upon chemical substitution and/or varying environmental conditions, which have been given a preliminary study in recent years. Thus the thermal evolution of structural properties has been investigated for a set of rare-earth gallates and their solid solutions. A strong anisotropy of thermal expansion has been observed in $LnGaO_3$ (Ln = La, Ce, Pr and Nd) orthogallates [7–10]. Furthermore, in $PrGaO_3$ an anisotropic negative thermal

[8] Author to whom any correspondence should be addressed.

expansion and even volumetric contraction of the lattice occurred at low temperatures [10, 11]. Similar trends have also been found in $Pr_{1-x}La_xGaO_3$ ($x = 0.61$, 0.81) solid solutions [12]. Note that no evident indications for a negative thermal expansion were detected in $LaGaO_3$, $CeGaO_3$, $NdGaO_3$ and $Ln'_xLn_{1-x}GaO_3$ solid solutions without praseodymium.

In order to explain the observed uniqueness of the Pr ion in the $LnGaO_3$ matrix, comprehensive studies using various methods of structure determination [7, 10], Raman scattering [7] and specific heat measurements [13] as well as theoretical simulations [14] have been performed. All these studies indirectly indicate that the crystal field splitting of the ground-state multiplet of the Pr^{3+} ions can presumably be the reason for the observed anomalous thermal expansion of $PrGaO_3$. A very similar anomalous behaviour has already been observed in perovskite-type rare-earth aluminates [15, 16] and perovskite-like $TmCaAlO_4$ [17]. Note that the unusual sequence (for perovskites) of phase transformations was observed in $PrAlO_3$ and $CeAlO_3$ and solid solutions based on them [18, 19], which might have the same origin.

A comprehensive study of the effect of praseodymium doping on the temperature evolution of LnO_{12} and GaO_6 coordination polyhedra in $LnGaO_3$ seems essential to elucidate the physical origin and the related structural features of the negative thermal expansion in rare-earth gallates containing praseodymium. Unfortunately, the formation of twins limits the use of the single crystal diffraction technique for structure determination; therefore, the crystal structure evolution was solely studied by powder diffraction. This work is a continuation of our systematic studies on structural properties [16] and domain structures [20, 21] of rare-earth perovskite-like gallates, aluminates and their solid solutions. Here we report results of *in situ* powder diffraction experiments using synchrotron and neutron radiation on $Pr_{1-x}Nd_xGaO_3$ and $LaGaO_3$ as a reference material.

2. Experimental details

Single crystals of $LaGaO_3$ and $Pr_{1-x}Nd_xGaO_3$ ($x = 0$, 0.25, 0.5, 0.75 and 1) were grown by the Czochralski method at the Institute of Physics (Warsaw, Poland). Details of the applied growth technique can be found elsewhere [22, 23]. Pieces of single crystalline ingots were crushed, ground and homogenized in size.

High-resolution diffraction experiments using synchrotron radiation were carried out on $Pr_{1-x}Nd_xGaO_3$ compositions with $x = 0.25$, 0.5, 0.75 on the powder diffractometer at beamline B2 at HASYLAB/DESY (Hamburg, Germany) [24]. Synchrotron diffraction data for rare-earth orthogallates ($LaGaO_3$, $PrGaO_3$ and $NdGaO_3$) were taken from our previous reports [7, 10]. All measurements were performed in Debye–Scherrer geometry. The quartz capillaries of diameter 0.3 mm were filled in air with powdered samples, shortened in lengths to 35 mm and then sealed. A modified closed-cycle He-cryostat [25] from Cryophysics™, equipped with a silicon diode as the temperature sensor and a PID control circuit via a LakeShore™ temperature controller was utilized for experiments with synchrotron radiation. The use of a capillary spinner ensured an appropriate averaging of crystallite orientation. In order to reduce absorption, a short wavelength of 0.502 06 Å was chosen from the 'white' synchrotron energy spectrum using a Si(111) double flat-crystal monochromator. The wavelength was determined from eight reflection positions of a LaB_6 reference material (NIST SRM 660a). The measurements at fixed temperatures (12–298 K temperature range) were performed in the sequence of increasing temperature. Data collection was carried out using the on-site readable position-sensitive image-plate detector OBI [26] in the 2θ-range of 6°–60°.

Elastic coherent neutron scattering experiments were performed on $NdGaO_3$, $Nd_{0.50}Pr_{0.50}GaO_3$ and $PrGaO_3$ samples at the Institut Laue Langevin (Grenoble, France) on the high-resolution diffractometer D2B [27]. Monochromatic neutrons ($\lambda = 1.595$ Å) were obtained at a 135° take-off using the 335 reflection of a vertically focused composite Ge monochromator. The vertical position-sensitive multidetector (300 mm effective height) consisting of 128 ^{3}He tubes and covering an angular span of 160° 2θ was used for data collection. Each sample (of about 1 cm^3 in volume) was filled into a thin-wall (0.15 mm) vanadium can of diameter 8 mm and then mounted in the top-loading closed-cycle refrigerator. Helium-4 was used as a heat transmitter. The instantaneous temperature was measured using two Cernox™ thin film resistance cryogenic temperature sensors and controlled by a temperature controller from LakeShore™. Two-dimensional powder diffraction data were collected at fixed temperatures in the range of 12–295 K. Data reduction was performed using the LAMP package.

Neutron powder diffraction studies on $LaGaO_3$ were performed on the SPODI powder diffractometer at the research reactor FRM-II (Garching b. München, Germany) [28] with an experimental setup and data collection times very similar to those at D2B.

The Rietveld and structure independent (Le Bail) refinements were carried out using the software package FullProf [29]. The peak profile shape was described by a pseudo-Voigt function. The background of the diffraction pattern was fitted using a linear interpolation between selected data points in non-overlapping regions. In order to deduce the evolution of lattice parameters the synchrotron data were treated via the full profile decomposition (Le Bail) technique, whereas the full profile Rietveld method was applied for the analysis of the neutron data. The scale factor, lattice parameter, fractional coordinates of atomic sites and their isotropic displacement parameters, zero angular shift, profile shape parameters and half width (Caglioti) parameters were varied during the fitting. For $NdGaO_3$, $Nd_{0.50}Pr_{0.50}GaO_3$ and $PrGaO_3$ it was found that the refinement of anisotropic thermal displacement parameters gives significant improvement of fits, which can probably be related to the more pronounced distortions from an ideal cubic perovskite structure in comparison to lanthanum gallate.

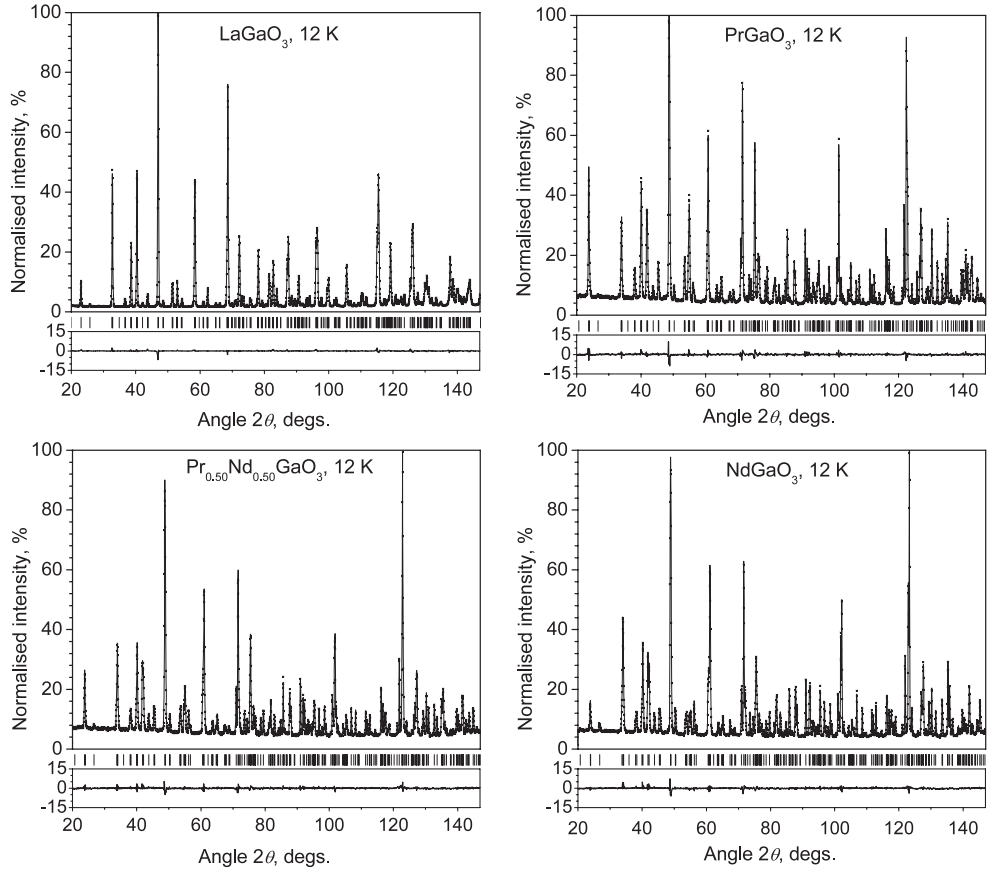

Figure 1. Results of Rietveld refinements for neutron powder diffraction data at 12 K for $LaGaO_3$ (SPODI powder diffractometer, $\lambda = 1.548$ Å) and $Pr_{1-x}Nd_xGaO_3$ ($x = 0$, 0.50, 1.00) (D2B powder diffractometer, $\lambda = 1.595$ Å). Experimental data are shown by points, lines denote calculated profiles and lower plots their difference. Calculated positions of Bragg reflections are shown by vertical tick marks.

3. Results and discussion

A preliminary inspection of the obtained powder diffraction patterns indicated that only reflections in agreement with the $GdFeO_3$ type of structure are present. This structure type (space group *Pbnm*, tilt system $a^-a^-c^+$ in the Glazer's notation [30]) has been found to be stable in the whole temperature range (12–300 K). The best Rietveld fits were obtained with those parameters listed in tables A.1–A.4 whilst the graphical results of the Rietveld refinements for $LaGaO_3$, $PrGaO_3$, $Pr_{0.50}Nd_{0.50}GaO_3$ and $NdGaO_3$ at 12 K are shown in figure 1.

The $GdFeO_3$ type of structure is the most often occurring structural type in the perovskite family and its description can be found elsewhere [16]. The orthorhombic perovskite lattice expands anisotropically with temperature, where elongation in various directions usually fulfils the relation $\Delta c > \Delta a > \Delta b$. The temperature dependences of lattice parameters for $LaGaO_3$ and $Pr_{1-x}Nd_xGaO_3$ ($x = 0$, 0.25, 0.50, 0.75 and 1.00) solid solutions are shown in figure 2, from which one can notice good qualitative agreement between neutron and synchrotron data.

A comparison of the temperature evolution of the lattice parameters in the *b* direction indicates essential differences: in $PrGaO_3$ the value of the *b* lattice parameter at 12 K is higher than the respective one at 300 K, i.e. the previously reported negative thermal expansion in the *b*-direction of the $PrGaO_3$ lattice is confirmed by the neutron experiment and is still persistent in $Pr_{0.50}Nd_{0.50}GaO_3$. Synchrotron diffraction revealed an even more complicated temperature behaviour of the *b* lattice parameter in $Pr_{0.25}Nd_{0.75}GaO_3$ and $Pr_{0.75}Nd_{0.25}GaO_3$ solid solutions: those temperature dependences have a sigmoidal shape, indicating the competitive evolution of various interaction mechanisms upon temperature variation. Furthermore, the magnitude of the negative thermal expansion has been found to be directly proportional to the amount of praseodymium in the $Pr_{1-x}Nd_xGaO_3$ solid solution. The temperature dependence of cell size in the [010] direction of $NdGaO_3$ shows a sigmoidal shape similar to $TmAlO_3$ [16, 31], whereas $LaGaO_3$ displays normal thermal expansion.

Assuming the Grüneisen constant γ and bulk modulus K to be temperature independent, the thermal evolution of the unit cell volume within the first order Grüneisen approximation can be described as follows [32]:

$$V(T) = V_0 + \frac{\gamma}{K_T}U(T) = V_0 + \frac{\gamma}{K_T}\left[9Nk_BT\left(\frac{T}{\theta_D}\right)^3\int_0^{\theta_D/T}\frac{x^3}{e^x-1}\,dx\right], \quad (1)$$

where U is the internal energy of the crystal, k_B is the Boltzmann constant, N is the number of atoms in the unit

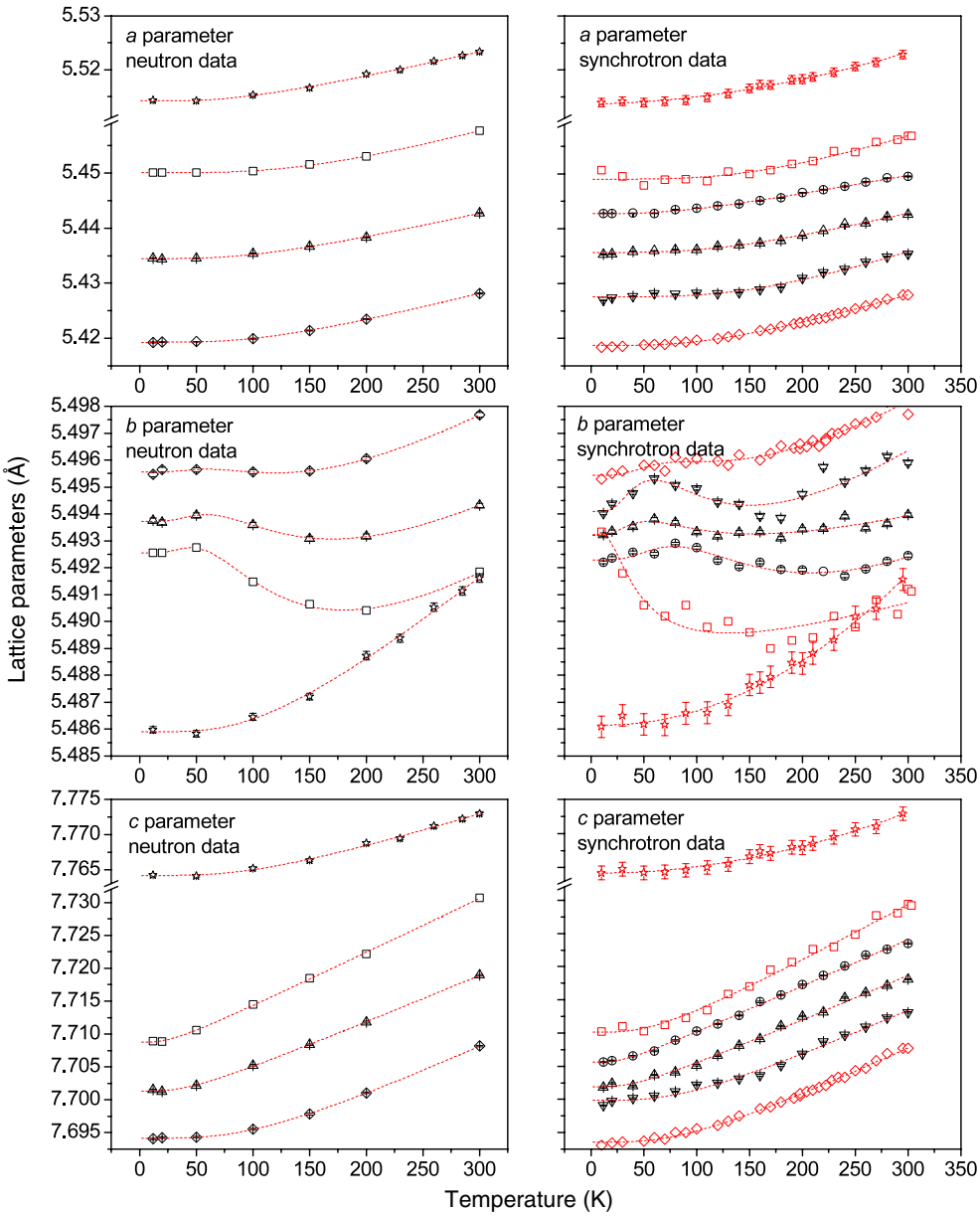

Figure 2. Temperature dependences of the lattice parameters in $LaGaO_3$ (☆), $PrGaO_3$ (□), $Pr_{0.75}Nd_{0.25}GaO_3$ (○), $Pr_{0.50}Nd_{0.50}GaO_3$ (△), $Pr_{0.25}Nd_{0.75}GaO_3$ (▽) and $NdGaO_3$ (◇). Synchrotron data for $LaGaO_3$, $PrGaO_3$ and $NdGaO_3$ were taken from [7, 10]. Dashed lines are results of nonlinear fitting of equation (4) to *a*, *b* and *c* lattice parameters.

cell ($N = 20$), θ_D is the Debye temperature and V_0 denotes the hypothetical cell volume at zero temperature. Vočadlo *et al* [33] discovered that the use of the Debye approximation for the internal energy as U in equation (1) provides a reasonable description for the cell volumes of FeSi and, just recently, Fortes *et al* [34] found that the lattice parameters (and not only the cell volume) of α-$MgSO_4$ can be fitted by a modified equation (1)

$$l(T) = l_0 + x_1 U(T), \tag{2}$$

where l corresponds to a, b or c lattice parameters, l_0 denotes the hypothetical lattice parameter at zero temperature and x_1 is the fitting parameter (in the case of using cell volumes it becomes a meaning of γ/K_T). However, equation (2) did not reproduce the negative thermal expansion which occurred in the *b*-direction of the β-$MgSO_4$ lattice. As is well known, the total thermal expansion coefficient, similar to heat capacity, is an additive property, i.e. usually consisting of different contributions—lattice, magnetic, electronic etc. Therefore, one more term, describing the lattice contraction, was introduced

$$l(T) = l_0 + x_1 U(T) + x_2 U_2(T), \tag{3}$$

where the x_2 fitting parameter has to be strictly negative, i.e. $x_2 < 0$, as the Grüneisen constant is only a parameter which can possess negative values in the definition of thermal expansion coefficient. This approach is often used in literature; thus it was successfully applied in [13] for determination of crystal electric field contribution to thermal expansion in

$PrGaO_3$. To describe U_2 one can use a single mode at fixed frequency, corresponding to a fixed Einstein temperature θ_E [34]. Thus equation (3) for the fitting of lattice parameters and cell volume takes the final form

$$l(T) = l_0 + x_1 \left[9Nk_BT \left(\frac{T}{\theta_D} \right)^3 \int_0^{\theta_D/T} \frac{x^3}{e^x - 1} dx \right] + x_2 \left[\frac{3Nk_B\theta_E}{\exp(\theta_E/T) - 1} \right], \quad (4)$$

where first and second terms in the square brackets correspond to the internal energy within Debye and Einstein approximations, respectively. Least-square fits to measured lattice parameters and cell volume were performed and the best agreement was obtained with parameters listed in the second half of table 1. The relatively poor data statistics causes large standard deviations and the overall nonlinear fit quality has been found to be more appropriate for neutron data in comparison to those derived from experiments with synchrotron radiation (see the R parameters in table 1). The better accuracy of neutron data can be explained by the improved counting statistics in neutron experiments, especially at high 2θ, as well as by the greater amount of sample and the improved average of crystallites over the irradiated sample. Therefore, from now on only neutron data will be considered.

As lanthanum gallate displays positive thermal expansion upon heating, lattice parameters were fitted by equation (4) using the Debye formula only. One can notice the same order of magnitude for x_1 and θ_D parameters for all directions, determined from the anisotropic expansion of the lattice. For parameters describing the cell volume, x_1 has the physical meaning of the γ/K ratio. Angel *et al* [35] determined the isothermal bulk modulus K_T in $LaGaO_3$ to 172.4 GPa, which gives 1.139 for the Grüneisen parameter. Despite the fact that perovskite-type rare-earth gallates cannot be perfectly described within the Debye approximation, such an estimation of the Grüneisen parameter is in good agreement with recent semiclassical simulations of lanthanum gallate [14], giving $K_T = 182.7$ GPa, $\gamma = 1.433$ and $\theta_D = 553$ K, respectively.

The a, c lattice parameters as well as the cell volume of $PrGaO_3$ were fitted by equation (2), whereas a description of the anomalous behaviour of the cell parameter in the b-direction requires the inclusion of an Einstein term with a negative Grüneisen scale. Significant correlations occurred between the x_1 and x_2 parameters, which caused instabilities in the refinement of the model. Therefore, the optimum value for x_2 was adjusted manually until the best agreement was received with $x_2 = -5.634 \times 10^{-13}$. In contrast to lanthanum gallate the differences in x_1 and θ_D parameters for the distinct crystallographic directions are more pronounced. This indicates not only that the b lattice parameter of praseodymium gallate exhibits an anomalous behaviour, but that the whole lattice does, even despite the positive thermal expansion coefficient. The same treatment technique has also been applied for $Pr_{0.50}Nd_{0.50}GaO_3$, where a very similar (but less pronounced) behaviour occurred.

As no obvious anomalies in the temperature evolution of $NdGaO_3$ lattice parameters were detected, their analyses were similar to those performed for lanthanum gallate, i.e. only a Debye term was used. A surprisingly high scattering of x_1 and θ_D parameters was observed after the fitting of the a, b and c lattice parameters. Furthermore, the obtained θ_D for the b direction was too high ($\theta_D = 2073$ K) and indicated a much lower thermal expansion coefficient. Indeed the thermal elongation in the b-direction of the $NdGaO_3$ lattice is obviously smaller than the one in $LaGaO_3$ and the $b(T)$ dependence in $NdGaO_3$ shows positive expansion with sigmoidal rather than exponential shape. To simulate this behaviour, the treatment applied for $b(T)$ in $PrGaO_3$ and $Pr_{0.50}Nd_{0.50}GaO_3$ was used, i.e. fitted to equation (4) with both Debye and Einstein terms for internal energy. As one can see, the inclusion (table 1, parameter b') of Einstein's term reduced θ_D to 463 K and resulted in a significant improvement of the fit.

Thus the model based on the Debye term only can be fitted to thermal behaviour of $LaGaO_3$, whereas a proper description of the anomalous behaviour in $PrGaO_3$, $Pr_{0.50}Nd_{0.50}GaO_3$ and $NdGaO_3$ requires the inclusion of Einstein's term with $x_2 < 0$, describing lattice contraction. The characteristic frequency of Einstein's oscillator (in terms of its energy) has been found to be very similar $E_E = k_BT_E \approx 22.1$, 24.9 and 25.3 meV for $PrGaO_3$, $Pr_{0.50}Nd_{0.50}GaO_3$ and $NdGaO_3$, respectively. The observed energy of Einstein's oscillator correlates very well with the $\Gamma_3 = 21.5$ meV level of a Pr ion in the $PrGaO_3$ matrix and with $\Gamma_2 = 22.5$ meV of Nd in $NdGaO_3$, determined from inelastic neutron spectroscopy by Podlesnyak *et al* [36, 37]. This is an indication of a phonon coupling to the crystalline electric field states of the 4f electrons. In this case different types of anomalies (contraction in $PrGaO_3$ and sigmoidal increase in $NdGaO_3$) can probably be related to the specific energy level schemes of Nd^{3+} and Pr^{3+} ions in the $LnGaO_3$ matrix.

In addition to the anomalous behaviour of the lattice parameters, an isomorphic substitution on the rare-earth site has an effect on the coordination polyhedra as well. An accurate determination of the thermal evolution of the coordination polyhedra requires an extended bond length analysis, better described based on a pseudo-cubic asymmetric unit, close to the ideal perovskite cell instead of the conventional orthorhombic one. In contrast to the ideal cubic prototype of the perovskite structure (space group $Pm\bar{3}m$) this pseudo-cubic cell with $Z = 1$ has a monoclinic distortion $a_p = b_p \neq c_p$ and $90^0 = \alpha = \beta \neq \gamma$ (see figure 3), i.e. the cube is stretched along its small diagonal in the a–b plane. The lattice parameters a_p, c_p and γ_p of such an asymmetric unit can be derived from the orthorhombic ones a, b and c as $a_p = \sqrt{a^2 + b^2}/2$, $c_p = c/2$ and $\gamma_p = 2\arctan(a/b)$. As one can see from figure 3 the Ln coordination polyhedron is formed by a 12-fold oxygen environment. In the $GdFeO_3$ type of structure, however, the oxygen cubooctahedron is built up of eight different Ln–O distances, i.e. 4 × Ln–O1 marked as (a)–(d) in figure 3 and 4 × 2 × Ln–O2 marked as (e)–(h) in figure 3.

The temperature evolution of rare-earth oxygen distances is shown in figure 4. The 'short' Ln–O distances (<2.9 Å, figures 4(a), (b), (e), (f), (g)) follow the rare-earth contraction. Thus $LaGaO_3$ has the longest Ln–O bonds, and the lengths smoothly decrease with increasing

Table 1. Results of nonlinear fit of equation (4) to lattice parameters a, b and c and cell volume. (Note: standard uncertainties were estimated using Monte Carlo technique on the basis of experimental errors for determination of the lattice parameters.)

Equation (4)	l_0 (Å)	$x_1 \times 10^{14}$	θ_D (K)	$x_2 \times 10^{14}$	θ_E (K)	R[a]
			$LaGaO_3$ (neutron data)			
a (Å)	5.5142 ± 0.0007	6.07 ± 1.84	376 ± 217	0	0	0.9989
b (Å)	5.4859 ± 0.0004	4.36 ± 1.49	471 ± 238	0	0	0.9989
c (Å)	7.7642 ± 0.0007	6.31 ± 2.37	434 ± 263	0	0	0.9985
V (Å)^3	234.87 ± 0.07	634.51 ± 202.65	418 ± 224	0	0	0.9988
			$LaGaO_3$ (synchrotron data)			
a (Å)	5.5139 ± 0.0004	6.31 ± 1.39	411 ± 142	0	0	0.9980
b (Å)	5.4862 ± 0.0003	4.53 ± 1.70	546 ± 235	0	0	0.9958
c (Å)	7.7643 ± 0.0007	6.70 ± 2.85	497 ± 270	0	0	0.9939
V (Å)^3	234.88 ± 0.05	660.69 ± 195.48	470 ± 188	0	0	0.9968
			$PrGaO_3$ (neutron data)			
a (Å)	5.4501 ± 0.0002	8.17 ± 2.15	709 ± 172	0	0	0.9998
b (Å)	5.4926 ± 0.0005	60.27 ± 2.30	402 ± 116	−56.34	256 ± 68	0.9987
c (Å)	7.7088 ± 0.0007	9.97 ± 0.82	100 ± 59	0	0	0.9999
V (Å^3)	230.8 ± 0.1	669.20 ± 422.05	447 ± 412	0	0	0.9972
			$PrGaO_3$ (synchrotron data)			
a (Å)	5.4491 ± 0.0013	9.04 ± 5.10	756 ± 426	0	0	0.9781
b (Å)	5.4932 ± 0.0021	48.98 ± 1.71	139 ± 113	−47.52	73 ± 77	0.9148
c (Å)	7.7101 ± 0.0016	10.48 ± 2.15	233 ± 164	0	0	0.9970
V (Å^3)	230.72 ± 0.12	848.25 ± 705.11	642 ± 562	0	0	0.9866
			$Pr_{0.75}Nd_{0.25}GaO_3$ (synchrotron data)			
a (Å)	5.4428 ± 0.0003	4.39 ± 0.83	340 ± 129	0	0	0.9984
b (Å)	5.4923 ± 0.0003	58.96 ± 4.28	521 ± 259	−55.58	353 ± 154	0.9277
c (Å)	7.7056 ± 0.0009	8.57 ± 0.77	109 ± 75	0	0	0.9991
V (Å^3)	230.36 ± 0.05	415.87 ± 59.58	179 ± 107	0	0	0.9984
			$Pr_{0.50}Nd_{0.50}GaO_3$ (neutron data)			
a (Å)	5.4345 ± 0.0004	5.97 ± 1.51	440 ± 165	0	0	0.9997
b (Å)	5.493 78 ± 0.0003	48.27 ± 1.38	436 ± 100	−44.88	289 ± 61	0.9985
c (Å)	7.7014 ± 0.0005	8.69 ± 0.82	161 ± 64	0	0	0.9997
V (Å^3)	229.94 ± 0.07	552.99 ± 224.09	337 ± 265	0	0	0.9985
			$Pr_{0.50}Nd_{0.50}GaO_3$ (synchrotron data)			
a (Å)	5.4357 ± 0.0005	5.98 ± 2.72	541 ± 292	0	0	0.9950
b (Å)	5.4932 ± 0.0004	62.86 ± 1.76	281 ± 200	−61.55	201 ± 136	0.8300
c (Å)	7.7019 ± 0.0012	8.26 ± 1.31	157 ± 122	0	0	0.9978
V (Å^3)	229.99 ± 0.06	472.74 ± 119.85	289 ± 176	0	0	0.9967
			$Pr_{0.25}Nd_{0.75}GaO_3$ (synchrotron data)			
a (Å)	5.4276 ± 0.0007	9.51 ± 7.68	758 ± 509	0	0	0.9910
b (Å)	5.4941 ± 0.0009	141.83 ± 4.71	312 ± 213	−137.92	222 ± 143	0.8860
c (Å)	7.6999 ± 0.0011	8.75 ± 2.98	357 ± 229	0	0	0.9952
V (Å^3)	226.38 ± 0.09	802.78 ± 221.57	653 ± 270	0	0	0.9956
			$NdGaO_3$ (neutron data)			
a (Å)	5.4193 ± 0.0002	6.93 ± 0.84	489 ± 79	0	0	0.9999
b (Å)	5.4956 ± 0.0002	15.75 ± 4.42	2073	0	0	0.9949
b' (Å)	5.4956 ± 0.0003	22.10 ± 3.08	463 ± 400	−18.77	294 ± 245	0.9979
c (Å)	7.6942 ± 0.0003	9.99 ± 1.07	429 ± 70	0	0	0.9999
V (Å^3)	229.15 ± 0.02	719.77912 ± 115.50	525 ± 105	0	0	0.9999
			$NdGaO_3$ (synchrotron data)			
a (Å)	5.4187 ± 0.0003	7.42 ± 1.08	513 ± 94	0	0	0.9986
b (Å)	5.4957 ± 0.0003	3.52 ± 3.80	909 ± 670	0	0	0.9673
b' (Å)	5.4954 ± 0.0003	44.46 ± 2.50	430 ± 277	−41.09	300 ± 185	0.9763
c (Å)	7.6935 ± 0.0005	9.18 ± 1.12	359 ± 84	0	0	0.9985
V (Å^3)	229.11 ± 0.03	686.52 ± 131.59	467 ± 124	0	0	0.9973

[a] The R parameter in this table corresponds to the coefficient of determination—a measure of quality of nonlinear regression—and it was determined as $R = \sqrt{1 - (\sum_i (y_i^{obs} - y_i^{cal})^2)/(\sum_i (y_i^{obs} - \langle y_i^{obs} \rangle)^2)}$.

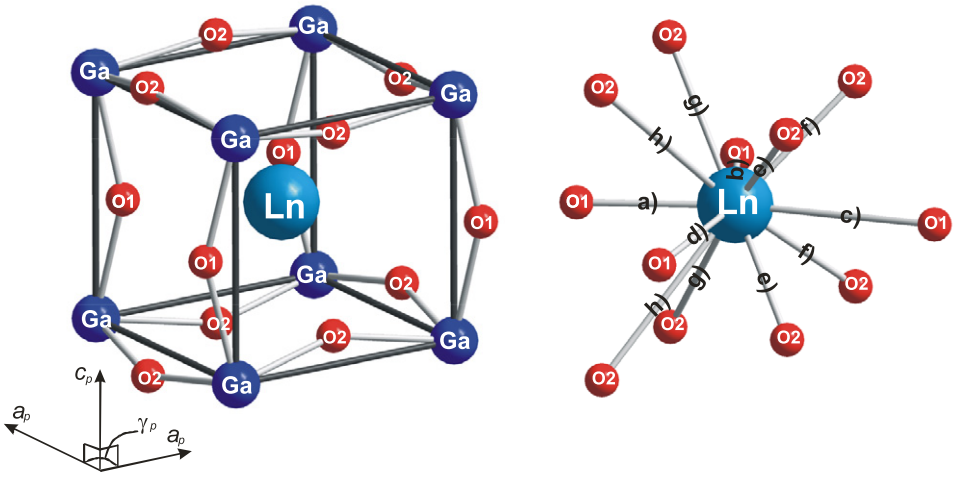

Figure 3. Pseudoprimitive perovskite cell in $LnGaO_3$ with $GdFeO_3$ structure type and LnO_{12} coordination polyhedron. Ln–O1 distances are marked in increased sequence as (a)–(d) and respective Ln–O2 distances are shown as (e)–(h).

Nd content in the $Pr_{1-x}Nd_xGaO_3$ solid solutions. Almost undistinguishable minima in the temperature dependences of the Ln–O1 (figure 4(a)) and Ln–O2 distances (figure 4(g)) occur at about 100 K in $PrGaO_3$, but their magnitude is very close to the standard deviation of bond length determination. No negative thermal expansion is observed for the 'short' Ln–O bonds in $LaGaO_3$, $Pr_{0.50}Nd_{0.50}GaO_3$ and $NdGaO_3$.

Two of the 'longer' Ln–O distances (figures 4(d) and (h)) display a behaviour in contrast to the expectations based on rare-earth contraction, i.e. the longest Ln–O distance was observed for $NdGaO_3$ and Ln–O bond lengths decrease in the sequence $Pr_{0.50}Nd_{0.50}GaO_3$, $PrGaO_3$ and $LaGaO_3$. The 'longer' Ln–O distances contribute only weakly to the Ln–O coordination polyhedra, and therefore this effect can be described by a reduction of the effective coordination number, which theoretically can reach 12, 10, 9 or 8 for the $GdFeO_3$ type of structure. This effect is especially obvious in temperature evolution of the Ln–O1 bond lengths (figure 4(c)), which are all very close to each other for $NdGaO_3$, $Pr_{0.50}Nd_{0.50}GaO_3$ and $LaGaO_3$. This observed similarity can indicate that the effective Ln–O coordination number in $NdGaO_3$, $Pr_{0.50}Nd_{0.50}GaO_3$ and $LaGaO_3$ is better described by 8. In a recent work [10], based on synchrotron diffraction, the coordination number of 8 was concluded for Pr in the temperature range 12–1000 K, whereas for temperatures above 1000 K a coordination number of 10 is preferred. More accurate neutron data indicated a slightly different temperature dependence of the considered Ln–O1 distance in $PrGaO_3$: at low temperatures the values are higher than for lanthanum gallate, neodymium gallate and $Pr_{0.50}Nd_{0.50}GaO_3$ solid solution. Upon heating this distance shows a small increase with a maximum at about 120 K and then decreases until approaching the values for the other compounds at 300 K. This observed behaviour might be related to an effective increase of the Ln–O coordination number in $PrGaO_3$ at low temperatures.

Such changes in the Ln–O coordination environment in praseodymium gallate can in principle cause a negative thermal expansion. On the other hand, the perovskite structure can be well described as a relatively rigid framework of corner-sharing, tilted and distorted octahedra. Even little differences in the Ln–O bonds will affect the tilting and distortion in the octahedral subsystem. Ga–Ga interatomic distances (which are equivalent to the a_p and c_p perovskite lattice parameters) are directly related (figure 5(a)) to the Ga–O interatomic distances L_1, L_2 (as arms) and interoctahedral angles Ga–O–Ga α_{oct} *via* the law of cosines.

Contraction of the Ga–Ga distance can be achieved by:

- a reduction of the interoctahedral angles Ga–O–Ga (rotational/tilting mechanism, figure 5(b)),
- compression of Ga–O interatomic distances (distortion mechanism, figure 5(c)),
- or a coexistence of these two mechanisms.

To elucidate the influence of octahedral tilt and distortion on negative thermal expansion in praseodymium gallium perovskite knowledge of the temperature evolution of Ga–O bond lengths in GaO_6 octahedra and of the Ga–O–Ga interoctahedral angles is required. Negative thermal expansion in $PrGaO_3$ has been found to be prominent in the b direction of the orthorhombic unit cell which corresponds to the a_p parameter of the smaller $Z = 1$ pseudoperovskite cell[9]. Thus only the Ga–O2–Ga angle and the Ga–O2 bond lengths need to be considered. The temperature dependence of the Ga–O1–Ga angle and the Ga–O1 distance have also been analysed for sake of completeness.

The temperature dependences of the Ga–O1–Ga and the Ga–O2–Ga tilt angles are shown in figures 6(a) and (b). Both tilt angles increase with temperature, and positive slopes of a linear fit for Ga–O1–Ga vary in the following sequence: $PrGaO_3 < Pr_{0.50}Nd_{0.50}GaO_3 \leqslant NdGaO_3 <$

[9] Not only the pseudoperovskite lattice parameter a_p but also the pseudoperovskite monoclinic angle γ_p of $PrGaO_3$ has to be included into considerations as well, since $\gamma_p = 2\arctan(a/b)$. In the current work the influence of γ_p can be neglected because its nonlinear temperature behaviour has been found fully consistent with those of $LaGaO_3$, $Pr_{0.50}Nd_{0.50}GaO_3$ and $NdGaO_3$.

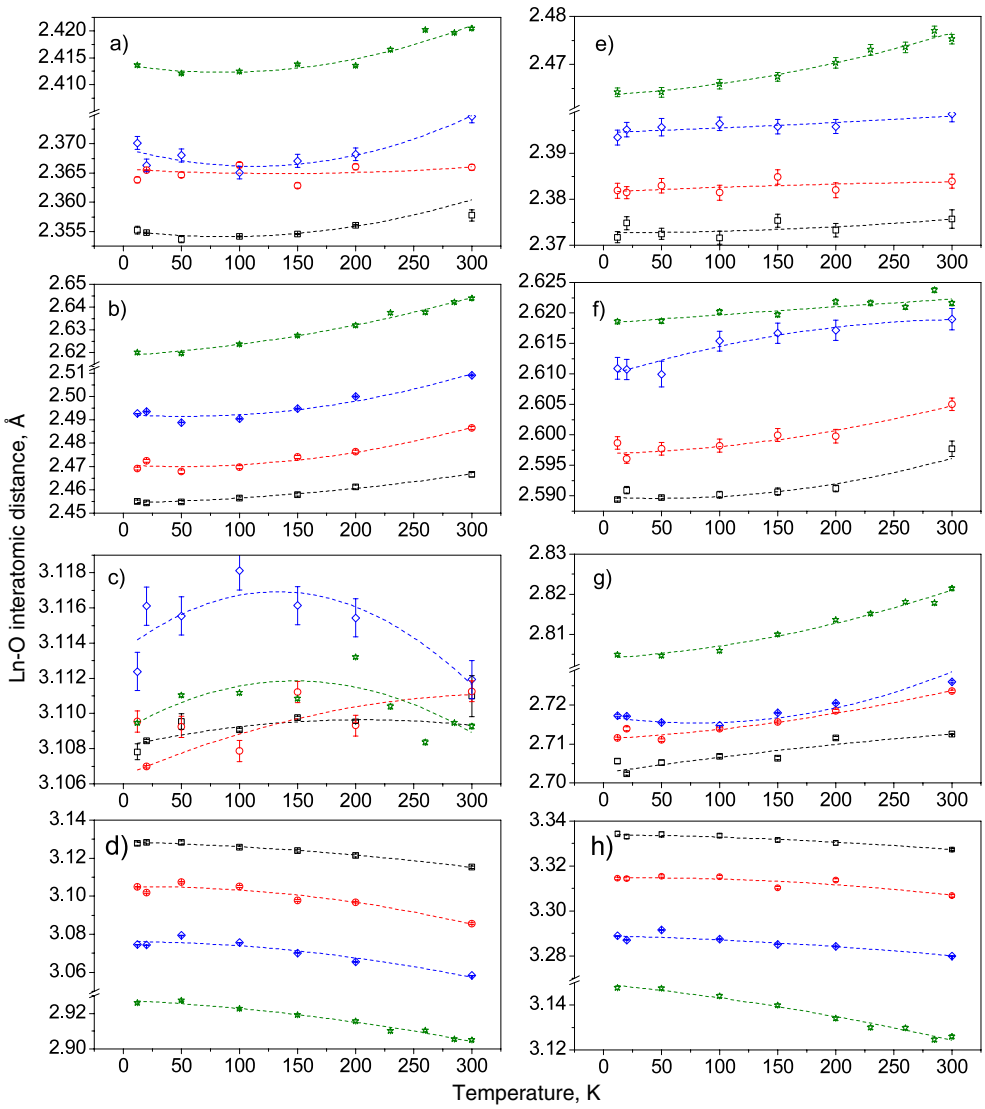

Figure 4. Temperature dependences of Ln–O1 ((a)–(d)) and Ln–O2 ((e)–(h)) interatomic distances in $LaGaO_3$ (★), $PrGaO_3$ (◊), $Pr_{0.50}Nd_{0.50}GaO_3$ (○) and $NdGaO_3$ (□). Dashed lines are shown as a guide for the eyes.

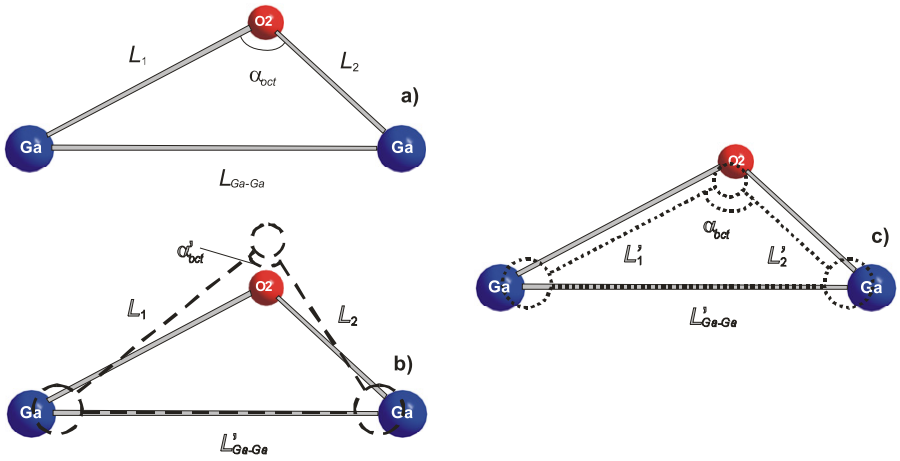

Figure 5. Illustration of the Ga–Ga interatomic distance as built on the framework of Ga–O2 ones (a) and various negative thermal expansion mechanisms in $GdFeO_3$ type of structure: rotational (b) and distortion (c).

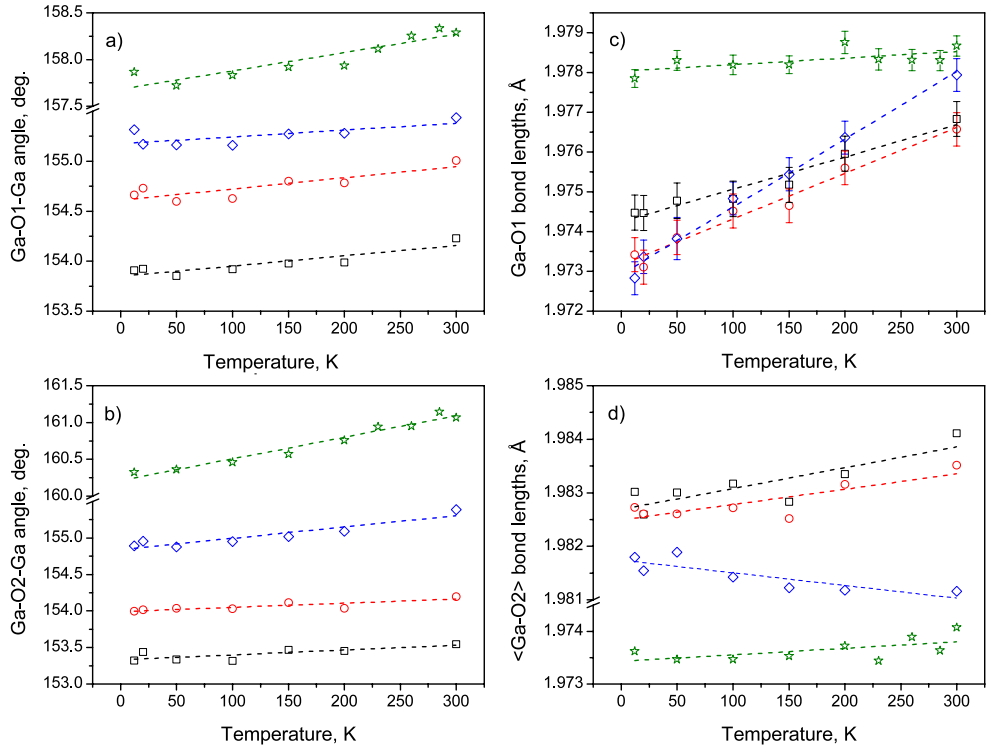

Figure 6. Temperature evolution of Ga–O1–Ga (a), Ga–O2–Ga (b) tilt angles and Ga–O1 (c), ⟨Ga–O2⟩ (d) interatomic distances in $LaGaO_3$ (☆), $PrGaO_3$ (◇), $Pr_{0.50}Nd_{0.50}GaO_3$ (○) and $NdGaO_3$ (□). Dashed lines are shown as guides for the eyes.

$LaGaO_3$, whereas for the Ga–O2–Ga tilt angle the sequence is $Pr_{0.50}Nd_{0.50}GaO_3 \leqslant NdGaO_3 < PrGaO_3 < LaGaO_3$. Positive slopes in the temperature dependence of the Ga–O2–Ga tilt angle rule out a significant role of the rotational mechanism for the negative thermal expansion of $PrGaO_3$.

The Ga–O1 interatomic distances (figure 6(c)) expand almost linearly with temperature, but their expansion changes drastically with chemical composition. $LaGaO_3$ displays the lowest expansion of the Ga–O1 bond within the series of investigated compounds, where positive slopes (linear thermal expansion coefficients) fulfil the sequence $LaGaO_3 < NdGaO_3 < Pr_{0.50}Nd_{0.50}GaO_3 < PrGaO_3$. In contrast to the Ga–O1 bonds, two kinds of Ga–O2 bonds exist in each GaO_6 octahedron. These bonds correlate with each other, so that high standard deviations result. In order to probe a possible role of the distortion mechanism for the negative thermal expansion, the evolution of the mean ⟨Ga–O2⟩ interatomic distances was analysed instead of the two distinct Ga–O2 bond lengths (see figure 6(d) for the temperature evolution). In combination with the increasing Ga–O2–Ga interatomic angles a positive expansion coefficient requires increasing mean ⟨Ga–O2⟩ distances with increasing temperature. This condition is accomplished in $LaGaO_3$, $NdGaO_3$ and $Pr_{0.50}Nd_{0.50}GaO_3$, whereas an obviously negative slope is detected in the temperature dependence of the mean ⟨Ga–O2⟩ distance for $PrGaO_3$ and the slope of ⟨Ga–O2⟩ increases in the following order: $PrGaO_3 < LaGaO_3 < Pr_{0.50}Nd_{0.50}GaO_3 < NdGaO_3$.

The estimation of bond length distortions (after Sasaki *et al* [38]) identifies $LaGaO_3$ among all compositions considered as the composition with the most regular GaO_6 octahedra, where irregularities increase with Nd content in $Pr_{1-x}Nd_xGaO_3$ ($x = 0.00$, 0.50 and 1.00). The stiffest octahedra (i.e. those with the lowest response to temperature changes) have been found in lanthanum gallate and change as $PrGaO_3 < Pr_{0.50}Nd_{0.50}GaO_3 < NdGaO_3 < LaGaO_3$, while the most severely distorted GaO_6 octahedra (and with the most pronounced temperature dependence of Ga–O bond lengths) are those in praseodymium gallate.

The observed differences in the coordination polyhedra of $LnGaO_3$ upon isomorphic substitution should be reflected in the behaviour of the thermal displacement parameters. In $PrGaO_3$, $Pr_{0.50}Nd_{0.50}GaO_3$ and $NdGaO_3$ the description of displacement parameters with a tensor of second rank gave a considerable improvement in the Rietveld refinement, whereas thermal vibrations of all atoms in lanthanum gallate were treated in the isotropic approximation. All determined $\langle u \rangle$ values (tables A.1–A.4) display the usual increase with temperature.

Typically in well ordered and close-packed systems the displacement parameters are proportional to the mass of the vibrating species. Thus the smallest magnitude of $\langle u \rangle$ was noticed for $LaGaO_3$, but then the mean displacement parameters increase in the row $NdGaO_3 < Pr_{0.50}Nd_{0.50}GaO_3 \leqslant PrGaO_3$ and in praseodymium gallate they become unusually large. A similar trend was observed for the diagonal elements u_{ii} ($i = 1, 2, 3$) of the Ln anisotropic displacement parameter tensor (a measure for the rotation of the principle axes system of thermal vibration against the crystal structure axes): $PrGaO_3 >$

$Pr_{0.50}Nd_{0.50}GaO_3$ > $NdGaO_3$ and in particular for Ga: $PrGaO_3$ > $Pr_{0.50}Nd_{0.50}GaO_3$ ⩾ $NdGaO_3$. Vibrational ellipsoids are stretched in the u_{22} direction (close to $7\bar{1}0$ in the $GdFeO_3$-type of structure), hence the eigenvalues of the displacement parameter tensor usually conform as $u_{22} \geqslant u_{33} > u_{11}$.

4. Summary

The temperature evolutions of $LaGaO_3$, $PrGaO_3$, $Pr_{0.50}Nd_{0.50}GaO_3$ and $NdGaO_3$ crystal structures were systematically studied using high-resolution neutron powder diffraction. In addition to previously reported [7, 10] data for $LaGaO_3$, $PrGaO_3$ and $NdGaO_3$ the temperature dependences of the lattice parameters in $Pr_{1-x}Nd_xGaO_3$ ($x = 0.25$, 0.50 and 0.75) solid solutions were studied by a high-resolution powder diffraction technique using synchrotron radiation.

The recently reported [7, 10, 11] negative thermal expansion in the *b*-direction of orthorhombic $PrGaO_3$ was confirmed by neutron diffraction. Furthermore, both neutron and synchrotron diffraction studies of praseodymium containing solid solutions $Pr_{1-x}Nd_xGaO_3$ revealed a negative thermal expansion in the *b*-direction, and its magnitude is proportional to the amount of praseodymium. Similar dependences have also been published for the $Pr_{1-x}La_xGaO_3$ ($x = 0.61$, 0.81) solid solutions [12], but have not been accounted for by these authors.

Semiclassical simulation indicated that perovskite-type rare-earth gallates cannot well be described as Debye-like solids (see [9, 14, 39]). The deviations between experimental data and Debye theory are, however, very similar for all considered $LnGaO_3$ compounds (Ln = La–Gd) [14]. The evaluation of obtained lattice parameters was performed on the basis of the first order Grüneisen approximation, where internal energy was parameterized using the Debye model. A fair performance of the model has been noticed for lanthanum gallate, whereas the simulation of the *b* lattice parameter in $LnGaO_3$ containing 4f elements (Pr and Nd) required the inclusion of a second term derived from the formulation of Einstein's oscillator and with a Grüneisen scale parameter $\gamma < 0$.

All eigenvalues of the $NdGaO_3$ thermal expansion tensor are positive in the whole temperature range studied. Nevertheless, the need for the inclusion of the Einstein's term is obvious, because of unusually low thermal expansion in the *b*-direction (as a consequence of high θ_D parameter). The observed anomalous behaviour of lattice parameters in $LnGaO_3$ perovskites and solid solutions containing either praseodymium or neodymium has the same origin, i.e. a crystal electric field–phonon coupling. Different terms and characters of their splitting under a crystal electric field can probably be the reason for the specific *b* versus *T* dependences in praseodymium and neodymium gallates.

An anomalous behaviour concerns not only the cell parameters, but also interatomic distances as well. Most pronounced anomalies of Ln–O bond lengths have been noticed for praseodymium gallium oxide. The presence of 'long' distances in the LnO_{12} cubooctahedron presupposes a weakening of interatomic forces and as a consequence a reduction of the 'real' coordination number. Based on the Ln–O1 interatomic distances (figure 4(c)) 'long' and 'short' bonds can be distinguished, and the 'real' coordination number in $LaGaO_3$, $Pr_{0.50}Nd_{0.50}GaO_3$ and $NdGaO_3$ was estimated to be 8. The same distance in $PrGaO_3$ shows a nonlinear behaviour at low temperatures, indicating possible changes in the Pr coordination, but at 300 K it becomes equal to those in $LaGaO_3$, $Pr_{0.50}Nd_{0.50}GaO_3$ and $NdGaO_3$.

On the other hand, the negative thermal expansions can be caused either by octahedral distortion or by octahedral tilt due to specific features of the $GdFeO_3$ structure type. The octahedral tilt mechanism is the typical reason for a negative thermal expansion in zeolite-like microporous solids, where 'negative thermal expansivity is the norm rather than the exception' [40]. The GaO_6 octahedra possess the highest and lowest rigidity (shape stiffness with respect to temperature) in lanthanum and praseodymium gallates, respectively. The mean ⟨Ga–O2⟩ bond decreases with temperature in $PrGaO_3$, indicating that the distortive mechanism is a structural response to the crystal electric field–phonon coupling, resulting in a change of the Pr coordination number. The eigenvalues of the thermal displacement parameter tensor in $PrGaO_3$ exhibit unusually high values, decreasing in the sequence $PrGaO_3$ > $Pr_{0.50}Nd_{0.50}GaO_3$ > $NdGaO_3$ > $LaGaO_3$.

At low temperatures a set of structural anomalies occur in $LnGaO_3$ with 4f Ln^{3+} ions and their solid solutions and can also be expected for other $LnMeO_3$ compounds, e.g. a very similar behaviour was already observed in rare-earth aluminates [16] and just recently in $TbMnO_3$ [41]. The most pronounced structural anomalies have been observed in praseodymium gallate, while the temperature dependences of the structural parameters (except the quite sensitive *b* lattice parameter) in neodymium gallate agree fairly well with the conventional behaviour of $LaGaO_3$. A lower praseodymium content in the $Ln_{1-x}Pr_xGaO_3$ solid solutions decreases the magnitude of the structural anomalies down to the detection limit (in terms of bond length determination). The current structural study was performed on the verge of accuracy for available methods of structure determination, therefore, a weak anomalous behaviour of $NdGaO_3$ and of solid solutions with small praseodymium content cannot be resolved. Future work on this topic should probably focus on inelastic neutron scattering, solid-state nuclear magnetic resonance and *ab initio* simulation techniques.

Acknowledgments

This work was partially supported by the Deutscher Akademischer Austauschdienst (DAAD), the German Federal Ministry of Education and Research (BMBF project 03FU7DAR, WTZ Grant UKR-04/007) and the Ukrainian Ministry of Education and Science (projects 'Segnet' and 'Tern').

Appendix. Structural parameters versus temperature

Temperature evolution of the structural parameters of $LaGaO_3$, $PrGaO_3$, $Pr_{0.50}Nd_{0.50}GaO_3$, $NdGaO_3$ as obtained from

Table A.1. Structural parameters of $LaGaO_3$.

		12 K	50 K	100 K	150 K	200 K	230 K	260 K	285 K	300 K
a (Å)		5.514 3(1)	5.5142(1)	5.5152(1)	5.5166(1)	5.5192(2)	5.5200(1)	5.5216(2)	5.5226(2)	5.5233(2)
b (Å)		5.486 0(1)	5.4858(1)	5.4865(1)	5.4872(1)	5.4887(2)	5.4894(1)	5.4905(2)	5.4911(2)	5.4916(2)
c (Å)		7.764 2(2)	7.7641(2)	7.7652(2)	7.7663(2)	7.7687(2)	7.7694(2)	7.7712(2)	7.7722(2)	7.7730(2)
La, 4c	x/a	−0.005 2(2)	−0.0054(2)	−0.0051(2)	−0.0050(2)	−0.0047(2)	−0.0047(2)	−0.0048(2)	−0.0045(2)	−0.0047(2)
	y/b	0.020 4(1)	0.0204(1)	0.0199(1)	0.0193(1)	0.0184(2)	0.0181(2)	0.0179(2)	0.0175(2)	0.0173(2)
	$\langle u \rangle$ (Å^2)	0.000 6(2)	0.0004(2)	0.0009(2)	0.0016(2)	0.0034(2)	0.0023(2)	0.0028(2)	0.0033(2)	0.0036(2)
Ga, 4b	$\langle u \rangle$ (Å^2)	0.000 4(2)	0.0005(2)	0.0008(2)	0.0008(2)	0.0018(2)	0.0002(2)	0.0009(2)	0.0009(2)	0.0008(2)
O1, 4c	x/a	0.068 4(2)	0.0689(2)	0.0685(2)	0.0683(2)	0.0682(2)	0.0677(2)	0.0672(2)	0.0670(2)	0.0671(2)
	y/b	0.492 2(2)	0.4920(2)	0.4924(2)	0.4924(2)	0.4923(3)	0.4930(3)	0.4928(3)	0.4932(3)	0.4932(3)
	$\langle u \rangle$ (Å^2)	0.001 9(2)	0.0017(3)	0.0021(2)	0.0025(2)	0.0034(3)	0.0035(3)	0.0032(3)	0.0037(3)	0.0040(3)
O2, 8c	x/a	−0.273 0(1)	−0.2730(1)	−0.2727(1)	−0.2721(1)	−0.2716(2)	−0.2713(2)	−0.2710(2)	−0.2707(2)	−0.2706(2)
	y/b	0.273 7(1)	0.2737(2)	0.2735(2)	0.2731(1)	0.2726(2)	0.2721(2)	0.2720(2)	0.2717(2)	0.2716(2)
	z/c	0.036 60(9)	0.0365(1)	0.0364(1)	0.0364(1)	0.0362(1)	0.0360(1)	0.0361(1)	0.0358(1)	0.0360(1)
	$\langle u \rangle$ (Å^2)	0.002 8(2)	0.0028(2)	0.0030(2)	0.0036(2)	0.0049(2)	0.0037(2)	0.0047(2)	0.0054(2)	0.0053(2)
R_p (%)		3.25	3.74	3.74	3.22	4.16	3.87	3.97	3.73	3.62
R_{wp} (%)		4.54	5.03	4.98	4.42	5.39	5.08	5.14	4.95	4.83

Table A.2. Structural parameters of $PrGaO_3$.

		12 K	20 K	50 K	100 K	150 K	200 K	300 K
a (Å)		5.450 10(8)	5.450 06(8)	5.450 13(10)	5.450 35(8)	5.451 53(8)	5.453 03(8)	5.457 73(9)
b (Å)		5.492 56(8)	5.492 56(8)	5.492 74(10)	5.491 47(8)	5.490 65(8)	5.490 41(8)	5.491 84(8)
c (Å)		7.708 91(12)	7.708 88(12)	7.710 55(16)	7.714 47(12)	7.718 49(12)	7.722 19(12)	7.730 69(13)
Pr, 4c	x/a	−0.007 2(5)	−0.007 0(5)	−0.007 2(6)	−0.006 7(5)	−0.006 8(5)	−0.007 1(5)	−0.007 7(5)
	y/b	0.037 8(3)	0.037 8(3)	0.038 5(3)	0.037 8(3)	0.037 1(3)	0.036 7(3)	0.035 7(3)
	u_{11} (Å^2)	0.004 5(7)	0.003 9(7)	0.004 4(9)	0.006 3(8)	0.007 1(8)	0.007 7(8)	0.007 3(9)
	u_{22} (Å^2)	0.009 1(8)	0.009 7(8)	0.009 1(10)	0.010 4(8)	0.011 3(7)	0.012 0(8)	0.013 5(8)
	u_{33} (Å^2)	0.009 2(7)	0.009 1(7)	0.009 4(10)	0.009 4(7)	0.009 6(8)	0.009 0(8)	0.012 4(9)
	u_{12} (Å^2)	−0.001 0(7)	−0.000 8(7)	−0.000 8(9)	−0.000 8(7)	−0.000 9(7)	0.000 0(8)	0.000 1(8)
	$\langle u \rangle$ (Å^2)	0.007 6(8)	0.007 6(8)	0.008(1)	0.008 7(8)	0.009 3(8)	0.009 6(8)	0.011 1(9)
Ga, 4b	u_{11} (Å^2)	0.002 4(5)	0.003 1(5)	0.003 1(7)	0.003 9(5)	0.004 6(5)	0.005 2(5)	0.005 6(5)
	u_{22} (Å^2)	0.008 1(4)	0.008 2(5)	0.007 3(6)	0.007 9(5)	0.008 3(5)	0.008 7(5)	0.009 9(5)
	u_{33} (Å^2)	0.007 2(6)	0.006 6(6)	0.007 5(7)	0.007 0(6)	0.007 1(6)	0.007 9(6)	0.009 5(7)
	u_{12} (Å^2)	−0.000 8(4)	−0.001 4(4)	−0.001 4(6)	−0.000 8(4)	−0.000 5(4)	−0.001 7(5)	−0.001 6(5)
	u_{13} (Å^2)	−0.002 8(5)	−0.001 7(5)	−0.002 1(7)	−0.003 1(7)	−0.003 8(7)	−0.003 6(8)	−0.003 8(9)
	u_{23} (Å^2)	0.000 1(4)	0.000 1(4)	−0.000 3(5)	−0.000 1(4)	0.000 6(4)	0.000 0(4)	0.000 4(4)
	$\langle u \rangle$ (Å^2)	0.005 9(5)	0.006 0(5)	0.006 0(7)	0.006 3(5)	0.006 7(5)	0.007 2(5)	0.008 3(6)
O1, 4c	x/a	0.075 7(3)	0.076 2(3)	0.076 2(4)	0.076 2(3)	0.075 9(3)	0.076 0(3)	0.075 6(3)
	y/b	0.484 1(3)	0.484 2(3)	0.484 0(3)	0.483 8(3)	0.484 0(3)	0.484 5(3)	0.485 0(3)
	u_{11} (Å^2)	0.006 2(7)	0.005 1(7)	0.005 0(9)	0.006 9(7)	0.006 0(7)	0.006 4(8)	0.008 2(8)
	u_{22} (Å^2)	0.011 4(7)	0.010 3(7)	0.011 2(9)	0.011 7(7)	0.012 3(7)	0.014 4(7)	0.016 6(8)
	u_{33} (Å^2)	0.006 6(7)	0.007 7(7)	0.007 5(10)	0.007 4(8)	0.008 3(8)	0.008 8(8)	0.009 5(9)
	u_{12} (Å^2)	−0.000 4(6)	−0.000 4(5)	−0.000 4(7)	−0.000 3(5)	−0.000 5(5)	−0.001 0(6)	−0.001 4(6)
	$\langle u \rangle$ (Å^2)	0.008 1(7)	0.007 7(7)	0.007 9(9)	0.008 7(7)	0.008 9(7)	0.009 9(8)	0.011 4(8)
O2, 8c	x/a	−0.287 52(18)	−0.287 46(18)	−0.287 7(2)	−0.287 55(18)	−0.287 34(18)	−0.287 26(18)	−0.286 81(19)
	y/b	0.287 99(17)	0.287 71(17)	0.288 0(2)	0.287 99(17)	0.288 01(16)	0.287 79(17)	0.287 14(18)
	z/c	0.041 06(13)	0.041 02(14)	0.041 01(17)	0.040 74(13)	0.040 69(14)	0.040 59(14)	0.040 15(16)
	u_{11} (Å^2)	0.006 3(4)	0.006 0(4)	0.006 1(5)	0.006 5(4)	0.006 7(4)	0.007 7(4)	0.008 6(4)
	u_{22} (Å^2)	0.009 1(4)	0.009 7(4)	0.009 1(5)	0.010 0(4)	0.010 0(4)	0.010 2(4)	0.012 3(4)
	u_{33} (Å^2)	0.007 8(4)	0.007 9(5)	0.008 0(6)	0.008 1(4)	0.009 2(4)	0.009 6(5)	0.011 4(5)
	u_{12} (Å^2)	0.000 2(4)	0.000 0(4)	−0.000 1(5)	−0.000 1(4)	−0.000 2(4)	−0.000 7(4)	−0.001 7(5)
	u_{13} (Å^2)	0.000 0(4)	−0.000 4(4)	0.000 1(5)	−0.000 2(4)	0.000 1(4)	−0.000 2(4)	0.000 4(4)
	u_{23} (Å^2)	−0.001 4(4)	−0.001 9(4)	−0.000 9(6)	−0.001 4(4)	−0.001 0(4)	−0.001 3(4)	−0.001 1(5)
	$\langle u \rangle$ (Å^2)	0.007 7(4)	0.007 9(4)	0.007 8(5)	0.008 2(4)	0.008 6(4)	0.009 2(4)	0.010 8(4)
R_p (%)		4.08	4.15	4.56	4.06	3.98	4.01	4.18
R_{wp} (%)		5.39	5.41	6.77	5.37	5.28	5.30	5.51

Table A.3. Structural parameters of $Pr_{0.50}Nd_{0.50}GaO_3$.

		12 K	20 K	50 K	100 K	150 K	200 K	300 K
a (Å)		5.434 51(9)	5.434 36(9)	5.434 56(9)	5.435 37(9)	5.436 67(9)	5.438 36(9)	5.442 76(8)
b (Å)		5.493 75(9)	5.493 69(9)	5.493 95(9)	5.493 59(9)	5.493 09(9)	5.493 17(9)	5.494 32(8)
c (Å)		7.701 51(13)	7.701 27(13)	7.702 22(13)	7.705 26(13)	7.708 38(14)	7.711 80(13)	7.718 96(12)
Nd/Pr, 4c	x/a	−0.008 5(4)	−0.008 8(3)	−0.008 8(4)	−0.009 0(4)	−0.008 0(4)	−0.008 6(4)	−0.007 9(4)
	y/b	0.041 0(2)	0.040 93(20)	0.041 27(20)	0.040 8(2)	0.040 4(2)	0.040 2(2)	0.038 8(2)
	u_{11} (Å^2)	0.003 7(6)	0.002 5(6)	0.003 4(6)	0.004 1(6)	0.005 2(6)	0.004 8(6)	0.005 4(6)
	u_{22} (Å^2)	0.007 2(6)	0.008 2(6)	0.007 5(6)	0.009 0(6)	0.008 3(6)	0.009 8(6)	0.012 8(6)
	u_{33} (Å^2)	0.005 3(6)	0.005 1(6)	0.005 5(6)	0.006 0(6)	0.007 1(7)	0.006 4(7)	0.007 6(6)
	u_{12} (Å^2)	−0.001 2(6)	−0.000 5(6)	−0.000 6(6)	−0.000 9(6)	−0.000 3(6)	−0.000 2(6)	−0.001 3(6)
	$\langle u \rangle$ (Å^2)	0.005 4(6)	0.005 2(6)	0.005 4(6)	0.006 3(6)	0.006 9(6)	0.007 0(6)	0.008 6(6)
Ga, 4b	u_{11} (Å^2)	0.003 3(5)	0.003 5(5)	0.003 9(5)	0.004 8(5)	0.005 4(6)	0.005 9(6)	0.007 0(5)
	u_{22} (Å^2)	0.008 3(5)	0.008 4(5)	0.008 6(5)	0.009 1(5)	0.010 2(5)	0.011 0(5)	0.010 6(5)
	u_{33} (Å^2)	0.003 8(6)	0.004 3(6)	0.004 7(6)	0.004 8(6)	0.004 0(6)	0.005 8(6)	0.006 3(6)
	u_{12} (Å^2)	0.000 5(5)	−0.000 8(5)	−0.000 5(5)	−0.000 1(5)	−0.000 4(6)	−0.000 2(6)	0.000 2(5)
	u_{13} (Å^2)	−0.000 5(6)	−0.000 7(6)	−0.000 8(6)	−0.001 6(7)	−0.000 9(7)	−0.001 8(7)	−0.000 8(8)
	u_{23} (Å^2)	0.000 5(4)	0.000 9(4)	0.000 7(4)	0.000 3(4)	0.001 0(4)	0.001 2(4)	0.000 1(4)
	$\langle u \rangle$ (Å^2)	0.005 1(5)	0.005 4(5)	0.005 7(5)	0.006 2(6)	0.006 6(6)	0.007 6(6)	0.008 0(6)
O1, 4a	x/a	0.077 6(3)	0.077 5(3)	0.077 8(3)	0.077 7(3)	0.077 3(3)	0.077 4(3)	0.076 8(3)
	y/b	0.482 3(3)	0.482 8(3)	0.482 2(3)	0.482 1(3)	0.482 8(3)	0.482 9(3)	0.483 5(3)
	u_{11} (Å^2)	0.007 0(7)	0.007 3(7)	0.007 9(7)	0.008 0(7)	0.008 2(7)	0.009 0(8)	0.010 4(7)
	u_{22} (Å^2)	0.009 2(8)	0.010 0(8)	0.009 0(8)	0.010 4(8)	0.010 7(8)	0.011 8(8)	0.012 2(8)
	u_{33} (Å^2)	0.007 3(8)	0.007 3(8)	0.006 1(8)	0.007 3(8)	0.009 0(9)	0.008 4(9)	0.009 1(8)
	u_{12} (Å^2)	0.000 6(6)	0.000 5(6)	−0.000 3(6)	0.001 0(6)	0.000 3(6)	0.000 2(6)	0.000 1(6)
	$\langle u \rangle$ (Å^2)	0.007 9(8)	0.008 2(8)	0.007 7(8)	0.008 5(8)	0.009 3(8)	0.009 7(8)	0.010 6(8)
O2, 8c	x/a	−0.289 1(2)	−0.289 1(2)	−0.289 3(2)	−0.289 3(2)	−0.288 7(2)	−0.288 8(2)	−0.288 1(2)
	y/b	0.289 82(18)	0.289 41(18)	0.289 61(18)	0.289 48(18)	0.289 24(18)	0.289 43(19)	0.289 12(18)
	z/c	0.042 28(15)	0.042 41(14)	0.042 15(15)	0.042 22(15)	0.042 33(15)	0.042 43(16)	0.042 37(15)
	u_{11} (Å^2)	0.007 1(4)	0.006 8(4)	0.007 5(4)	0.007 8(4)	0.008 2(4)	0.007 9(4)	0.009 6(4)
	u_{22} (Å^2)	0.007 6(4)	0.007 6(4)	0.008 1(4)	0.007 9(4)	0.008 1(4)	0.009 5(4)	0.010 7(4)
	u_{33} (Å^2)	0.005 3(5)	0.006 6(5)	0.006 5(5)	0.007 2(5)	0.007 3(5)	0.007 7(5)	0.009 2(5)
	u_{12} (Å^2)	−0.001 2(4)	−0.002 0(4)	−0.001 7(4)	−0.002 0(4)	−0.002 6(5)	−0.003 0(5)	−0.003 1(4)
	u_{13} (Å^2)	−0.000 7(4)	0.000 3(4)	−0.000 7(4)	−0.000 7(5)	0.000 3(5)	0.001 2(5)	0.001 3(5)
	u_{23} (Å^2)	−0.000 8(5)	−0.000 5(5)	−0.000 3(5)	−0.000 1(5)	−0.000 6(5)	−0.001 2(5)	−0.001 1(5)
	$\langle u \rangle$ (Å^2)	0.006 7(4)	0.007 0(4)	0.007 4(4)	0.007 6(4)	0.007 9(4)	0.008 4(4)	0.009 9(4)
R_p (%)		3.75	3.71	3.71	3.75	3.67	3.75	3.32
R_{wp} (%)		4.89	4.79	4.87	4.85	4.82	4.81	4.34

treatment of neutron data by the Rietveld method. Here and below (tables A.1–A.4) the space group is $Pbnm$ (No. 62). The structural data were modelled for Ln and O1 ions occupying the 4c position with $z/c = 1/4$, Ga occupies position 4b [1/2, 0, 0]. Numbers in parentheses give statistical errors in the last significant digit.

Table A.4. Structural parameters of $NdGaO_3$.

		12 K	20 K	50 K	100 K	150 K	200 K	300 K
a (Å)		5.419 25(8)	5.419 32(8)	5.419 37(8)	5.419 92(8)	5.421 43(8)	5.423 50(8)	5.428 17(9)
b (Å)		5.495 47(8)	5.495 65(9)	5.495 64(8)	5.495 56(8)	5.495 59(8)	5.496 05(8)	5.497 68(9)
c (Å)		7.694 07(12)	7.694 26(12)	7.694 33(12)	7.695 56(12)	7.697 86(12)	7.701 06(11)	7.708 17(13)
Nd, 4c	x/a	−0.010 0(2)	−0.009 9(3)	−0.009 9(2)	−0.009 8(3)	−0.009 7(3)	−0.009 8(3)	−0.009 2(3)
	y/b	0.043 39(15)	0.043 68(16)	0.043 45(15)	0.043 16(16)	0.043 26(16)	0.042 41(15)	0.041 70(16)
	u_{11} (Å^2)	0.002 9(5)	0.003 3(5)	0.004 2(5)	0.003 7(5)	0.004 6(5)	0.006 0(5)	0.006 5(5)
	u_{22} (Å^2)	0.004 5(4)	0.004 5(4)	0.004 7(4)	0.005 8(4)	0.006 5(4)	0.006 7(4)	0.008 6(5)
	u_{33} (Å^2)	0.003 8(5)	0.002 9(5)	0.003 7(5)	0.004 5(5)	0.004 7(5)	0.005 4(5)	0.007 6(5)
	u_{12} (Å^2)	0.000 3(5)	0.000 4(5)	0.000 4(5)	0.000 5(5)	0.000 3(5)	−0.000 9(5)	−0.000 8(5)
	$\langle u \rangle$ (Å^2)	0.003 7(4)	0.003 6(4)	0.004 2(4)	0.004 7(5)	0.005 3(5)	0.006 1(5)	0.007 6(5)
Ga, 4b	u_{11} (Å^2)	0.004 0(5)	0.004 9(5)	0.005 0(5)	0.005 6(5)	0.005 4(5)	0.004 7(5)	0.005 6(5)
	u_{22} (Å^2)	0.007 4(5)	0.007 5(5)	0.007 4(5)	0.007 1(5)	0.007 6(5)	0.008 0(5)	0.008 7(5)
	u_{33} (Å^2)	0.004 9(5)	0.004 5(5)	0.004 7(5)	0.005 3(6)	0.006 7(6)	0.006 5(5)	0.007 7(6)
	u_{12} (Å^2)	0.000 6(5)	0.000 1(5)	−0.000 1(5)	0.000 0(5)	0.000 3(5)	0.000 1(5)	0.000 1(5)
	u_{13} (Å^2)	0.001 7(5)	0.000 8(6)	0.000 8(5)	0.001 7(6)	0.001 2(6)	0.001 9(6)	0.000 0(6)
	u_{23} (Å^2)	0.001 4(4)	0.000 6(4)	0.000 8(4)	0.000 0(4)	−0.000 1(4)	0.000 1(4)	−0.000 3(4)
	$\langle u \rangle$ (Å^2)	0.005 4(5)	0.005 6(5)	0.005 7(5)	0.006 0(5)	0.006 6(5)	0.006 4(5)	0.007 3(5)
O1, 4c	x/a	0.080 0(3)	0.080 0(3)	0.080 2(3)	0.080 0(3)	0.079 9(3)	0.079 8(3)	0.079 1(3)
	y/b	0.481 2(3)	0.481 4(3)	0.481 2(3)	0.481 3(3)	0.481 7(3)	0.481 4(3)	0.481 8(3)
	u_{11} (Å^2)	0.005 0(6)	0.005 0(6)	0.005 4(6)	0.005 3(6)	0.005 8(6)	0.006 7(6)	0.007 9(7)
	u_{22} (Å^2)	0.009 5(7)	0.010 3(7)	0.011 1(7)	0.012 3(8)	0.012 8(7)	0.011 4(7)	0.013 9(8)
	u_{33} (Å^2)	0.007 8(7)	0.007 8(7)	0.008 3(7)	0.008 3(7)	0.008 4(7)	0.008 2(7)	0.009 6(8)
	u_{12} (Å^2)	−0.001 5(5)	−0.001 1(5)	−0.001 6(5)	−0.001 7(5)	−0.000 9(5)	−0.001 3(5)	−0.001 5(5)
	$\langle u \rangle$ (Å^2)	0.007 4(7)	0.007 7(7)	0.008 3(7)	0.008 6(7)	0.009 0(7)	0.008 8(7)	0.010 5(7)
O2, 8c	x/a	−0.291 0(2)	−0.291 0(2)	−0.290 9(2)	−0.290 7(2)	−0.290 5(2)	−0.290 59(20)	−0.290 4(2)
	y/b	0.290 88(17)	0.290 92(18)	0.290 95(17)	0.291 04(18)	0.290 79(17)	0.290 25(17)	0.290 30(18)
	z/c	0.043 01(14)	0.042 62(14)	0.042 97(14)	0.043 08(14)	0.042 81(14)	0.043 06(14)	0.042 82(15)
	u_{11} (Å^2)	0.006 3(4)	0.006 4(4)	0.006 7(4)	0.006 8(4)	0.007 4(4)	0.008 1(4)	0.009 7(4)
	u_{22} (Å^2)	0.007 5(4)	0.007 4(4)	0.007 1(4)	0.007 6(4)	0.008 8(4)	0.009 8(4)	0.011 0(4)
	u_{33} (Å^2)	0.007 9(5)	0.007 0(5)	0.007 2(4)	0.007 1(5)	0.008 5(5)	0.008 8(5)	0.009 8(5)
	u_{12} (Å^2)	−0.000 7(4)	−0.000 9(4)	−0.000 9(4)	−0.000 8(4)	−0.000 9(4)	−0.000 8(4)	−0.001 2(4)
	u_{13} (Å^2)	0.000 6(5)	0.001 0(5)	0.001 4(4)	0.000 6(5)	0.000 9(5)	0.001 5(5)	0.000 5(5)
	u_{23} (Å^2)	−0.001 2(4)	−0.001 0(5)	−0.000 8(4)	−0.000 7(5)	−0.000 9(5)	−0.000 7(5)	−0.001 3(5)
	$\langle u \rangle$ (Å^2)	0.007 3(4)	0.006 9(4)	0.007 0(4)	0.007 2(4)	0.008 2(4)	0.008 9(4)	0.010 2(4)
R_p (%)		3.71	3.71	3.65	3.74	3.64	3.53	3.58
R_{wp} (%)		4.86	4.91	4.79	4.84	4.73	4.60	4.62

References

[1] Mamutin V V, Toropov A A, Kartenko N F, Ivanov S V, Wagner A and Monemar B 1999 *Mater. Sci. Eng.* B **59** 56–9

[2] Mogro-Campero A, Turner L G, Hall E L, Garbauskas M F and Lewis N 1989 *Appl. Phys. Lett.* **54** 2719–21

[3] Sandstrom R L, Giess E A, Gallagher W J, Segmüller A, Cooper E I, Chisholm M F, Gupta A, Shinde S and Laibowitz R B 1988 *Appl. Phys. Lett.* **53** 1874–6

[4] Petric A and Huang P 1996 *Solid State Ion.* **92** 113–7

[5] Ishihara T, Furutani H, Arikawa H, Honda M, Akbay T and Takita Y 1999 *J. Electrochem. Soc.* **146** 1643

[6] Liu Z, Cong L, Huang X, Lü Z and Su W 2001 *J. Alloys Compounds* **314** 281–5

[7] Savytskii D, Vasylechko L, Senyshyn A, Matkovskii A, Baehtz C, Sanjuan M L, Bismayer U and Berkowski M 2003 *Phys. Rev.* B **68** 024101

[8] Vasylechko L O and Senyshyn A T 2004 *Visnyk Lviv Polytech. Natl Univ., Electron.* **513** 3 (in Ukrainian)

[9] Senyshyn A, Vasylechko L, Knapp M, Bismayer U, Berkowski M and Matkovskii A 2004 *J. Alloys Compounds* **382** 84–91

[10] Vasylechko L, Pivak Ye, Senyshyn A, Savytskii D, Berkowski M, Borrmann H, Knapp M and Paulmann C 2005 *J. Solid State Chem.* **178** 270–8

[11] Marti W, Fischer P, Altorfer F, Scheel H J and Tadin M 1994 *J. Phys.: Condens. Matter* **6** 127–35

[12] Aleksiyko R, Berkowski M, Byszewski P, Dabrowski B, Diduszko R, Fink-Finowicki J and Vasylechko L O 2001 *Cryst. Res. Technol.* **36** 789–800

[13] Senyshyn A, Schnelle W, Vasylechko L, Ehrenberg H and Berkowski M 2007 *J. Phys.: Condens. Matter* **19** 156214

[14] Senyshyn A, Ehrenberg H, Vasylechko L, Gale J D and Bismayer U 2005 *J. Phys.: Condens. Matter* **17** 6217–34

[15] Vasylechko L, Trots D, Senyshyn A and Lukasiewicz T 2006 *Hasylab Annual Report* vol 1, pp 605–6

[16] Vasylechko L, Senyshyn A and Bismayer U 2009 *Handbook on the Physics and Chemistry of Rare-Earths* vol 39, ed K A Gschneidner Jr, J-C G Bünzli and V K Pecharsky (Amsterdam: Elsevier) p 113

[17] Vasylechko L, Prots Yu, Trots D, Senyshyn A, Baehtz C and Knapp M 2004 *Hasylab Annual Report* vol 1, pp 179–80

[18] Carpenter M A, Howard C J, Kennedy B J and Knight K S 2005 *Phys. Rev.* B **72** 024118

[19] Vasylechko L, Senyshyn A, Trots D, Niewa R, Schnelle W and Knapp M 2007 *J. Solid State Chem.* **180** 1277–90
[20] Savytskii D I, Trots D M, Vasylechko L O, Tamura N and Berkowski M 2003 *J. Appl. Crystallogr.* **36** 1197–203
[21] Savytskii D, Senyshyn A, Matkovskii A, Vasylechko L, Wieteska K, Wierzchowski W, Lukasiewics T and Bismayer U 2003 *Z. Kristallogr.* **218** 17
[22] Berkowski M, Fink-Finowicki J, Byszewski P, Diduszko R, Kowalska E, Aleksiyko R, Piekarczyk W, Vasylechko L O, Savytskii D I, Perchuc L and Kapusniak J 2001 *J. Cryst. Growth* **222** 194–201
[23] Berkowski M, Fink-Finowicki J, Piekarczyk W, Perchuc L, Byszewski P, Vasylechko L O, Savytskii D I, Mazur K, Sass J, Kowalska E and Kapusniak J 2000 *J. Cryst. Growth* **209** 75–80
[24] Knapp M, Baehtz C, Ehrenberg H and Fuess H 2004 *J. Synchrotron Radiat.* **11** 328–34
[25] Ihringer J and Küster A 1993 *J. Appl. Crystallogr.* **26** 135–7
[26] Knapp M, Joco V, Baehtz C, Brecht H H, Berghaeuser A, Ehrenberg H, von Seggern H and Fuess H 2004 *Nucl. Instrum. Methods Phys. Res.* A **521** 565–70
[27] Convert P, Hansen T, Oed A and Torregrossa J 1997 *Physica* B **241** 195–7
[28] Hoelzel M, Senyshyn A, Gilles R, Boysen H and Fuess H 2007 *Neutron News* **18** 23–6
[29] Roisnel T and Rodriguez-Carvajal J 2001 *Mater. Sci. Forum* **378–381** 118
[30] Glazer A M 1972 *Acta Crystallogr.* B **28** 3384–92
[31] Senyshyn A, Vasylechko L, Trots D M and Knapp M 2005 *HASYLAB Annual Report* vol 1, pp 433–5
[32] Wallace D C 1972 *Thermodyamics of Crystals* (New York: Wiley)
[33] Vočadlo L, Knight K S, Price G D and Wood I G 2002 *Phys. Chem. Miner.* **29** 132–9
[34] Fortes A D, Wood I G, Vočadlo L, Brand H E A and Knight K S 2007 *J. Appl. Crystallogr.* **40** 761–70
[35] Angel R J, Zhao J, Ross N L, Jakeways C V, Redfern S A T and Berkowski M 2007 *J. Solid State Chem.* **180** 3408–24
[36] Podlesnyak A, Rosenkranz S, Fauth F, Marti W, Scheel H J and Furrer A 1994 *J. Phys.: Condens. Matter* **6** 4099–106
[37] Podlesnyak A, Rosenkranz S, Fauth F, Marti W, Furrer A, Mirmelstein A and Scheel H J 1993 *J. Phys.: Condens. Matter* **5** 8973–82
[38] Sasaki S, Prewitt C T and Liebermann R C 1983 *Am. Mineral.* **68** 1189–98
[39] Senyshyn A, Oganov A R, Vasylechko L, Ehrenberg H, Bismayer U, Berkowski M and Matkovskii A 2004 *J. Phys.: Condens. Matter* **16** 253–65
[40] Lightfoot P, Woodcock D A, Maple M J, Villaescusa L A and Wright P A 2001 *J. Mater. Chem.* **11** 212–6
[41] Berggold K, Baier J, Meier D, Mydosh J A, Lorenz T, Hemberger J, Balbashov A, Aliouane N and Argyriou D N 2007 *Phys. Rev.* B **76** 094418